Progress In Electromagnetics Research, PIER 97, 141–158, 2009

EFFECTS OF FIBROGLANDULAR TISSUE DISTRIBUTION ON DATA-INDEPENDENT BEAMFORMING ALGORITHMS

M. O'Halloran, M. Glavin, and E. Jones

Electronic and Electrical Engineering
National University of Ireland Galway
Ireland

Abstract—The effects of the fibroglandular tissue distribution of the breast on data-independent microwave imaging algorithms are investigated in this paper. A data-independent beamformer is a beamformer whose weights do not depend on the array data and are chosen, based on a channel model, to compensate for path-dependent attenuation and phase effects. The effectiveness and robustness of data-independent UWB beamforming algorithms relies upon two specific characteristics of breast tissue at microwave frequencies: Firstly, that there exists a significant dielectric contrast between cancerous tissue and normal healthy breast tissue; secondly, that the propagation, attenuation and phase characteristics of normal tissue allow for constructive addition of the UWB returns using the Confocal Microwave Imaging (CMI) technique. However, two recent studies by Lazebnik et al. have highlighted a significant dielectric contrast between normal adipose and fibroglandular tissue within the breast. These results suggest a much more difficult imaging scenario where clutter due to fibroglandular tissue is a significant concern and that constructive addition of backscattered signals is potentially much more problematic than previously assumed. In this paper, three existing data-independent beamformers are tested on several different breast models, examining the effect of different fibroglandular tissue distribution on the performance of the data-independent imaging algorithms.

Corresponding author: M. O'Halloran (martin.ohalloran@gmail.com).

1. INTRODUCTION

In recent years, microwave imaging of the breast has been seen as one of the most promising alternatives to X-ray mammography for the early detection of breast cancer. Worldwide, the incidence of breast cancer has increased by 0.5% annually, with between 1.35 and 1.45 million new cases projected by 2010. Breast cancer mortality is on the decline in industrialized countries such as the United States, Canada, Germany, Austria and the United Kingdom and this decline can be attributed in no small part to increased breast cancer screening, and the early detection and treatment of the disease [1]. A comprehensive physical examination and regular self-examination are often successful in tumor detection while randomized clinical trials using X-ray mammography have been shown to detect tumors at an earlier stage and reduce disease-specific mortality. However, the significant limitations of X-ray mammography in terms of sensitivity and specificity are well documented, and the motivation for improved breast imaging modalities is clear [1]. The goal is to develop an imaging system that will reliably detect the presence and location of breast cancer at the earliest stage of development, when intervention is most effective.

Two criteria determine the effectiveness of any breast cancer screening methodology, specificity and sensitivity. Specificity is defined as the proportion of patients correctly identified as not having breast cancer. Conversely, sensitivity is defined as the proportion of patients correctly identified as having as breast cancer. Therefore, a good screening methodology must have both high sensitivity and specificity. If the screening technology determines the presence of a tumor, two further criteria become significant: The ability of the technology to localize the abnormalities within the breast for further examination or treatment, and the ability of the technology to accurately characterize the abnormality and help in the decision-making process. An ideal imaging technology would accomplish all these goals, and in addition, be inexpensive, practical, harmless and appealing to the patient. Microwave imaging has the potential to meet these goals.

Ultra-wideband (UWB) Radar imaging of the breast is based on the dielectric contrast between normal and cancerous tissue at microwave frequencies. The breast presents a relatively small volume, making it an attractive site for microwave imaging, and since the breast is primarily composed of adipose tissue, it is relatively penetrable to UWB signals. UWB imaging algorithms typically involve illuminating the breast with a UWB pulse, and then measuring the backscattered signals. The Confocal Microwave Imaging (CMI) approach is used

to process these backscattered signals to create a high resolution backscattered energy distribution map, where regions of high energy suggest the potential presence of cancerous tissue.

Based on several studies examining the dielectric properties of normal and cancerous breast tissue, UWB beamforming algorithms were developed based on the following set of assumptions:

- There is a significant dielectric contrast between normal and cancerous breast tissue.
- The breast is primarily dielectrically homogeneous.
- The dielectric properties of normal tissue is such that constructive addition of UWB backscattered signals is possible.

However, a much more recent study of the dielectric properties of adipose, fibroglandular and cancerous breast tissue has highlighted the dielectric heterogeneity of normal breast tissue [2, 3]. The dielectric properties of adipose tissue was found to be lower than any previously published data for normal tissue. Conversely, the dielectric properties of fibroglandular tissue was found to be significantly higher than any previously published data for normal breast tissue, and the dielectric contrast between this tissue and cancerous tissue was found to be as little as 10%. This heterogeneity of normal breast tissue had been considerably underestimated by previous studies, and presents a much difficult imaging scenario.

The performance and robustness of data-independent beamformers in the context of this increased dielectric heterogeneity has not yet been comprehensively examined. In this paper, three existing data-independent beamformers are examined and evaluated with respect to this heterogeneity. The remainder of the paper is organized as follows: Section 2 will examine the recently-established dielectric heterogeneity of normal breast tissue; Section 3 will describe the three data-independent beamformers tested; Section 4 will describe the test procedure and corresponding results; Finally, the conclusions and suggestions for future work are detailed in Section 5.

2. DIELECTRIC HETEROGENEITY OF NORMAL BREAST TISSUE

The dielectric properties of both normal and cancerous tissue have been the subject of many studies over the last thirty years, and the general findings are summarised here. Chaudhary [4], Surowiec [5] and Joines et al. [6] measured the dielectric properties of normal and cancerous breast tissues from 3 MHz and 3 GHz, 20 kHz to 100 MHz, and 50 MHz to 900 MHz respectively. These studies found a significant

dielectric contrast between normal and cancerous tissue. The measured permittivity and conductivity as established by Chaudhary, Surowiec and Joines et al. are shown in Figures 1, 2 and 3.

Campbell and Land [7] measured the complex permittivity of female breast tissue at 3.2 GHz, and once again noted a significant dielectric contrast between normal (fat tissue and all other breast tissue) and cancerous tissue. However, the study also suggested that

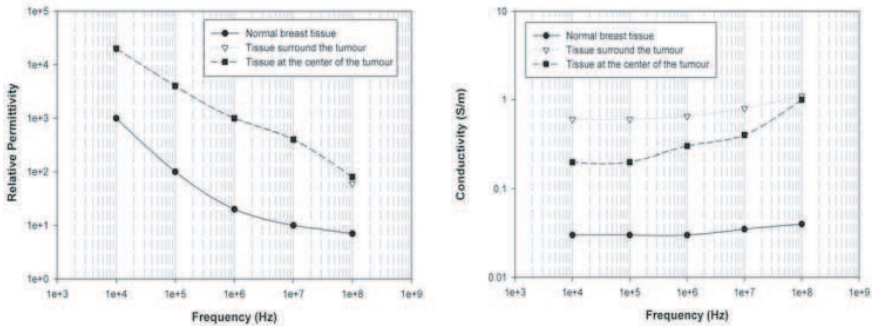

(a) (b)

Figure 1. The variation of (a) the relative permittivity, and (b) the conductivity of tumour tissue, the surrounding tissue, and peripheral tissue across the frequency band of 0.02 MHz and 100 MHz as reported by Surowiec et al. [5].

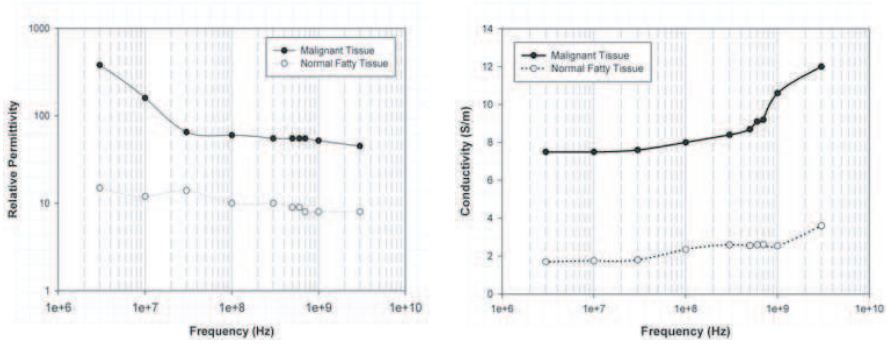

(a) (b)

Figure 2. The variation of the relative permittivity (a) and conductivity (b) of normal and malignant tissue between 3 MHz and 3 GHz as reported by Chaudhary et al. [4].

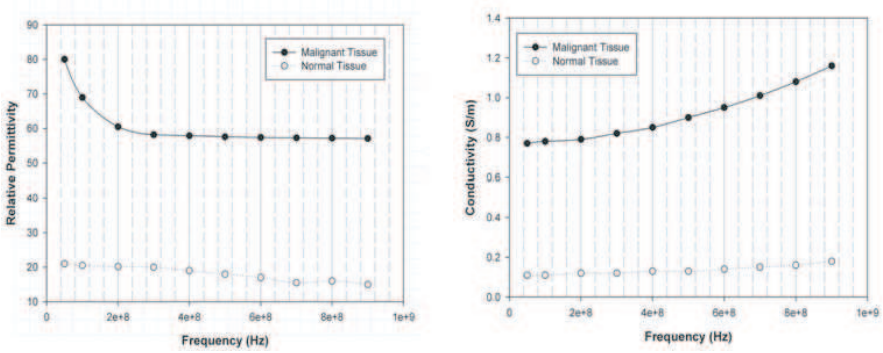

(a) (b)

Figure 3. The variation of (a) the relative permittivity, and (b) the conductivity of normal and malignant tissue between 50 MHz and 900 MHz as reported by Joines et al. [6].

Table 1. Dielectric properties of female breast tissue at 3.2 GHz as reported by Campbell and Land [7].

Tissue type	Relative Permittivity	Conductivity (S/m)	Water content (%)
Fatty tissue	2.8–7.6	0.54–2.9	11–31
Normal tissue	9.8–46	3.7–34	41–76
Benign tissue	15–67	7–49	62–84
Malignant tissue	9–59	2–34	66–79

Table 2. Average dielectric properties of female breast tissue at 900 MHz measured *in vivo* using an active microwave imaging system developed by Meaney et al. [8].

Patient	Age	Average Permittivity	Average Conductivity (S/m)
1	76	17.22±11.21	0.5892±0.3547
2	57	31.14±4.35	0.6902±0.3650
3	52	36.44±6.24	0.6869±0.3156
4	49	35.43±3.93	0.5943±0.3841
5	48	30.85±7.22	0.6350±0.3550

the range of dielectric properties of normal tissue was much greater than established in previous studies. These results are summarised in Table 1.

Furthermore, Meaney et al. measured the average permittivity and conductivity of cancer-free breast tissue using a clinical prototype of a tomographic microwave imaging system, the results of which are shown in Table 2. Once again, Meaney et al. [8] noted that the average permittivity values of normal tissue at 900 MHz were significantly higher than those previously published in Joines et al.'s *ex vivo* study [6]. Meaney et al. suggested that a correlation existed between the average permittivity values and the radiographic density of the tissue, since patients categorised radiographically as having high fat content tissue had an average permittivity value of 31, while patients categorised as having heterogeneously dense tissue had average relative permittivities between 35 and 36.

Finally, one of the most recent, and arguably most comprehensive examinations of the dielectric properties of normal and malignant tissue, was undertaken by Lazebnik et al. [2, 3]. One of the most significant differences between Lazebnik et al.'s first study and previous studies was the histological categorisation of the samples. Each sample under consideration was quantified in terms of the percentage of adipose, glandular and fibroglandular tissue present in the sample. In order to effectively summarise the data, Lazebnik et al. formed 3 groups of tissue:

(i) Group 1 contained all samples with 0–30% adipose tissue (99 samples).

(ii) Group 2 contained all samples with 31–84% adipose tissue (84

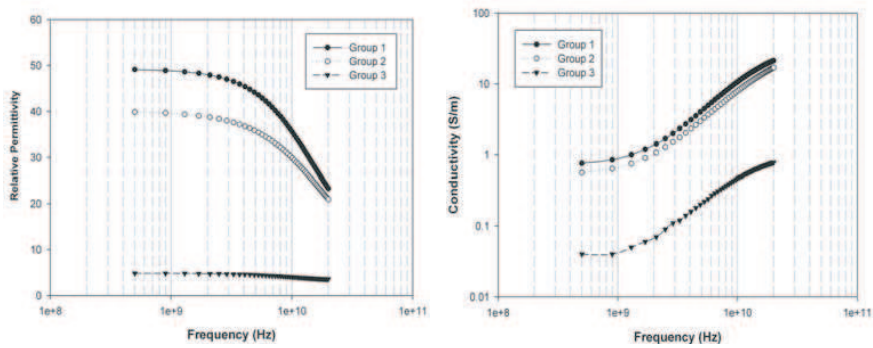

(a) (b)

Figure 4. The relative permittivity (a), and conductivity (b) of normal breast tissue as measured by Lazebnik et al. [2] over the frequency band 0.5 to 20 GHz. Group 1 represents 0–30% adipose tissue, group 2 represents 31–84% adipose and group 3 represents 85–100% adipose tissue.

samples).

(iii) Group 3 contained all samples with 85–100% adipose content (171 samples).

Median permittivity and conductivity curves were created by calculating the fitted values for each sample in the group at 50 equally spaced frequency points. Secondly, the median value at a particular frequency was calculated across all samples within a group. Finally, Cole-Cole equations were used to fit these median values. The Cole-Cole representations for permittivity and conductivity for each tissue group are shown in Figure 4. Lazebnik et al. compared the results of her study with the results of previous studies and her findings were as follows:

(i) Lazebnik et al.'s median dielectric curves (relative permittivity and conductivity) for group 3 tissue was lower than any previously published data for normal tissue, as shown in Figure 4. This tissue consists of between 85 and 100% adipose tissue.

(ii) Lazebnik et al.'s median dielectric curves (relative permittivity and conductivity) for group 1 tissue was higher than any previously published data for normal tissue. This tissue has a low adipose content between 0 and 30% (due to the high concentration of fibroglandular tissue).

(iii) With the exception of data published by Campbell and Land [7], the dielectric properties of breast tissue (both adipose and fibroglandular) spanned a much greater range of values than had been reported in smaller scale studies.

Lazebnik et al. attributed these differences to the large heterogeneity in normal breast tissue, as previously noted by Campbell and Land [7]. Lazebnik et al. suggested that the reason that this level of heterogeneity was not found in previous studies was the location from which samples of normal tissue were taken. In previous studies, the samples of normal tissue were taken from regions distinct from the tumour site, and since tumours typically occur in glandular tissue, these normal samples were likely to have a higher adipose content compared to the glandular tissue surrounding the tumour. Therefore, the dielectric heterogeneity of breast tissue was previous underestimated. Lazebnik et al. also concluded that the dielectric properties of breast tissue were primarily a function of the adipose content of the tissue. The effect of this heterogeneity on data-independent beamformers has yet to be comprehensively examined.

3. DATA-INDEPENDENT BEAMFORMING ALGORITHMS

In this section, three data-independent breast imaging algorithms are detailed, the Delay and Sum (DAS), the Improved Delay and Sum (IDAS), and the Delay, Multiply and Sum (DMAS) beamformer.

3.1. Delay and Sum Beamformer

The monostatic Delay and Sum beamformer was originally developed by Hagness et al. [9, 10], and extended to the multistatic case by Nilavalan et al. [11]. First, consider a voxel r_0 within the breast. In the multistatic DAS algorithm, the distance from each transmitting antenna to r_0 and back to the receiving antenna is calculated based on the average speed of propagation, and converted into time delays. These time delays are used to isolate the response from r_0 within each multistatic signal. These responses are summed and squared to calculate the intensity value associated with the point r_0, as shown in Equation (1)

$$I(r_0) = \left[\sum_{m=1}^{M} \sum_{n=1}^{M} B_{m,n}(\tau_{m,n}(r_0)) \right]^2 \tag{1}$$

where $B_{m,n}$ is the backscattered waveform transmitted from the mth antenna and received at the nth antenna and $\tau_{m,n}(r_0)$ is defined as follows:

$$\tau_{m,n}(r_0) = \frac{d_{m,n}}{s} \frac{1}{f} \tag{2}$$

where $d_{m,n}$ is the distance from the mth transmitting antenna to the point r_0 and back to the nth receiving antenna, f is the sampling frequency, and s is the average speed of propagation in breast tissue and is defined as follows:

$$s = \frac{c}{\sqrt{\epsilon_r}} \tag{3}$$

where ϵ_r is the relative permittivity of normal adipose tissue at the centre frequency of the UWB input signal and c is the speed of light. The synthetic focal point r_0 is then scanned throughout the breast and an image of the backscattered energy from within the breast is created.

3.2. Delay Multiply and Sum Beamformer

The Delay, Multiply and Sum algorithm [12] once again involves synthetically focusing the backscattered signals at a focal point within the breast, and then scanning this focal point throughout the

breast. The signals are time-aligned using the procedure described above. Following time-alignment, an additional pairing multiplication procedure is applied. This procedure involves pair-multiplying each multistatic signal with the other multistatic signals which have a common transmitting antenna. The multiplied signals are then summed and squared, and the intensity at the point r_0 is calculated.

3.3. Improved Delay and Sum Beamformer

The Improved Delay and Sum (IDAS) algorithm was developed by Klemm et al. [13]. The beamformer is based on the weighted Delay and Sum beamformer, with the weights compensating for both attenuation and radial spreading of the UWB pulse. The algorithm uses an extra weighting factor, based on the coherence of the backscattered responses at each synthetic focal point within the breast. For each point r_0, a plot of energy collected versus number of multistatic signals is created. This energy curve is normalised by multiplying the curve by $\frac{1}{1+\sigma_e}$, where σ_e is the standard deviation of the energy. Finally, a second-order polynomial is fitted to the normalised energy curve (ax^2+bx+c). The coefficient a is a measure of the coherence of the backscattered signals at the point r_0. The Quality Factor, QF, associated with point r_0 is assigned the value a, and the Improved Delay and Sum algorithm is then defined as follows:

$$I(r_0) = QF(r_0) \cdot \left[\sum_{m=1}^{M} \sum_{n=1}^{M} w(r_0) B_{m,n}(\tau_{m,n}(r_0)) \right]^2 \tag{4}$$

where $w(r_0)$ is the weighting factor associated with the point r_0.

4. TESTING AND RESULTS

In this section, the effects of different distributions of fibroglandular tissue within the breast on the performance of these data-independent beamformers is evaluated. The beamformers are tested on 2D Finite Difference Time Domain (FDTD)-generated backscattered signals from three breast phantoms with increasing levels of fibroglandular heterogeneity. Section 4.1 details the FDTD breast models used to generate the representative backscattered signals and the metrics used to evaluate the beamformers, while Section 5 describes the testing procedure and the corresponding results.

4.1. FDTD Models for Data Acquisition

Three numerical breast phantoms were created using the FDTD method, reflecting increasing levels of fibroglandular tissue within the breast. An accurate FDTD model must incorporate the appropriate geometrical properties of the breast, the heterogeneity and spatial distribution of the different constituent tissues within the breast, while also reflecting the most recent and most accurate dielectric properties. The models are that of a naturally flattened breast from a patient lying in the supine position. Therefore, in two dimensions, a sagittal slice of breast is considered with a planar conformal antenna array placed close to the skin. The antenna array consists of 14 elements modeled as electric-current sources, and are equally spaced on the surface of the skin along the horizontal span-axis from 1 cm to 9 cm. The antenna array is backed by a synthetic material matching the dielectric properties of skin. The adipose/fibroglandular tissue distribution within the breast is established by linearly mapping the regions of adipose and fibroglandular tissue from a high resolution T2 weighted MR image to the FDTD grid, as previously used by Li et al. [14]. The lighter regions within the breast represented fibroglandular tissue, while the darker regions represented adipose tissue. A simple thresholding algorithm was applied to the MRI scan to differentiate between the different regions of tissue, and then a linear transformation algorithm was used to map the tissue distribution in the MRI scan to the FDTD grid. This method was chosen since it preserved the highly correlated nature of fibroglandular tissue distribution in the breast, as opposed to the other methods that model the variance of dielectric properties as being randomly distributed.

Three FDTD models are created. The first model contains only adipose tissue and no fibroglandular tissue. This model acts as an "idea" imaging scenario for the beamformers and is a useful benchmark in determining the effects of fibroglandular tissue within the breast. The second model is based on an MRI slice taken at a distance from the areola and nipple, where the fibroglandular distribution is less significant. In this model, there are significant regions of fibroglandular tissue, but also regions of adipose tissue where no fibroglandular tissue is present. The third model is based on a sagittal slice close to the areola, where the fibroglandular tissue distribution is much more significant and presents a much more difficult imaging scenario. The three models are shown in Figure 5. The dielectric properties of adipose and fibroglandular tissue used in the FDTD models are based on Lazebnik et al.'s recent publications [2, 3]. Lazebnik et al. defined the 25th, 50th, and 75th percentile of the measured dielectric properties of adipose and fibroglandular as low, medium and high

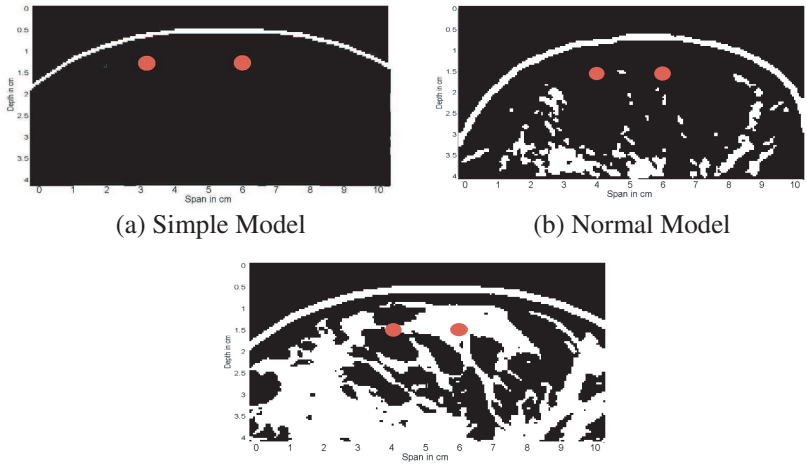

(a) Simple Model (b) Normal Model

(c) Dense Model

Figure 5. FDTD Models of the breast. The first model contains no fibroglandular tissue, the second contains a normal distribution and the third model is that of a dense breast where the fibroglandular tissue content is significant. Note: depth is measured on the vertical axis and span is measured on the horizontal axis.

values respectively. The dielectric properties used in the FDTD models described here are based on the median values. As previously described, Lazebnik et al. matched the frequency-dependence of the dielectric properties to Cole-Cole models. However, the frequency dependence of the dielectric properties of breast tissue is more readily incorporated into FDTD simulations using Debye parameters rather than Cole-Cole parameters, and therefore Debye parameters which provided an excellent fit to the Cole-Cole models across the frequency range of interest (100 MHz to 10 GHz) were derived empirically (similar Debye models have since been derived by Lazebnik et al. [15]).

The Debye parameters for skin are chosen to fit published data by Gabriel et al. [15, 16], while the Debye parameters for malignant tissue are those used by Bond et al. [17]. The Debye parameters for each type of tissue, along with the permittivity and conductivity at the centre frequency, are shown in Table 3.

The FDTD grid resolution, dx, is 0.5 mm and the time step dt is defined as 0.833 ps ($dt = \frac{dx}{2c}$). A specific location within the FDTD model is defined as follows: ($span$, $depth$). A 10 mm tumour is artificially introduced at two different positions within the model: (4.0, 1.5) and (6.0, 1.5). A scan involves sequentially illuminating the

breast model with a UWB pulse from each antenna, while recording the backscattered signal at all antennas. Since there are 14 antenna array elements, this results in 196 recorded multistatic signals. Before further processing, the signals are downsampled from 1200 GHz (the time step in the FDTD simulation) to 50 GHz. The input signal is a 150-ps differentiated Gaussian pulse, with a centre frequency of 7.5 GHz and a −3 dB bandwidth of 9 GHz. An idealized artifact removal algorithm, as previously described by Bond et al. [17] is used to remove the input signal and the reflection from the skin-breast interface. The artifact to be removed is established by measuring the backscattered signals from the first homogeneous FDTD model with no tumour present. These signals are then subtracted channel-by-channel from the with-tumour responses. Finally, since the input signal is a differentiated Gaussian pulse with a zero crossing at its centre point, the backscattered signal from any dielectric scatterer would also have a zero crossing at its centre point. In order to overcome this, the signals are integrated to produce a maximum at the centre point.

4.2. Metrics

Two metrics are used to determine the performance of the beamformers. The first metric is the Signal to Clutter ratio (S/C) which is defined as the ratio of the peak tumour response to the maximum clutter energy in the breast [19, 20]. The second metric is the Signal to Mean ratio (S/M) which is defined as the ratio of the peak tumour energy to the mean energy within the breast [12].

5. RESULTS

Six FDTD simulations were completed, with a tumour at two different locations across the three distribution models, as shown in Figure 5.

Table 3. Debye parameters for the FDTD model and dielectric properties of each tissue at the centre frequency of the input pulse.

Tissue	ϵ_r	χ_1	σ	t_0 (ps)	Relative Perm.	Cond. (S/m)
Skin	15.63	8.2	0.82	12.6	21.65	2.35
Tumor	7	47	0.15	7	49.2	6.1
Adipose (Medium)	3.20	1.65	0.035	16	4.30	0.38
Fibroglandular (Medium)	11.2	38	0.738	12	39.65	7.65

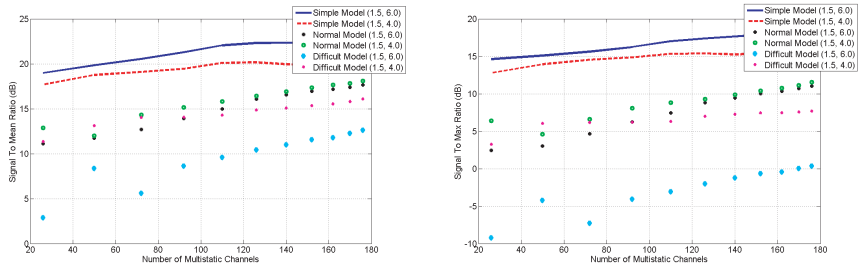

(a) Signal to Mean ratio (b) Signal to Clutter ratio

Figure 6. S/M and S/C ratio for Delay and Sum beamformer (DAS) across the simple, normal and dense fibroglandular distributions.

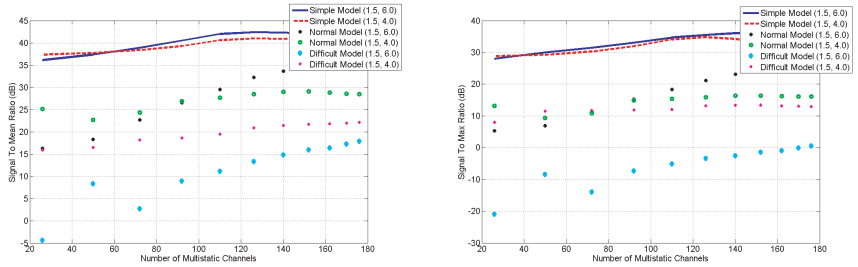

(a) Signal to Mean ratio (b) Signal to Clutter ratio

Figure 7. S/M and S/C ratio for Improved Delay and Sum beamformer (IDAS) across the simple, normal and dense fibroglandular distributions.

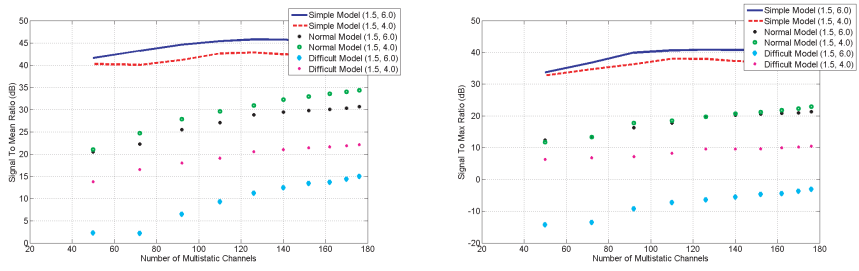

(a) Signal to Mean ratio (b) Signal to Clutter ratio

Figure 8. S/M and S/C ratio for Delay, Multiply and Sum beamformer (DMAS) across the simple, normal and dense fibroglandular distributions.

The DAS, DMAS and IDAS beamformers were each applied to the backscattered signals. The S/C and S/M ratios, plotted as a function of the number of multistatic channels used, for the simple Delay and Sum, Improved Delay and Sum, and Delay Multiply and Sum beamformers are shown in Figures 6, 7 and 8 respectively. In the simple distribution, the S/C and S/M generally increase with the number of multistatic channels used. This can be attributed to the accuracy between the assumed and actual propagation channel, allowing for the constructive addition of the multistatic signals.

Both the S/M and S/C ratios for all beamformers decrease significantly with increasing fibroglandular content within the breast. The effect of the increased fibroglandular tissue is also evident in the resultant images created by each multistatic beamformer, as shown in Figures 9, 10 and 11 (it should be noted that the associated dB scale varies with each image). The presence and location of the tumour is clearly visible in the simple model. In the normal fibroglandular model, the tumour is still visible, however there are also significant non-cancerous high energy regions due to the presence of fibroglandular tissue. Finally, the precise location of the tumour in the dense model is very difficult to correctly identify due to the large amount of fibroglandular tissue surrounding the tumour.

Significantly, while both the IDAS and DMAS beamformer considerably outperform the traditional DAS beamformer in terms of both S/M and S/C across the simple and normal distribution models, the improvement offered by these beamforming algorithms is appreciably less for the dense model, as shown in Table 4. The dielectric heterogeneity of normal breast tissue means that different multistatic signals propagate through tissue with different dielectric properties, making the constructive addition of backscattered signals much more problematic. The performance and robustness of both IDAS and DMAS beamformers algorithms are highly dependent on

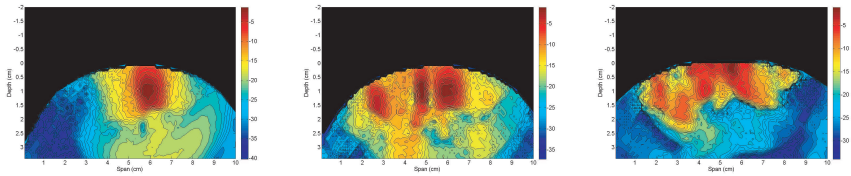

(a) Simple distribution (b) Normal distribution (c) Dense distribution

Figure 9. Images created by the Delay and Sum (DAS) beamformer for the simple, normal and dense fibroglandular tissue distributions, with a 5 mm tumour centered at location (1.5, 6.0).

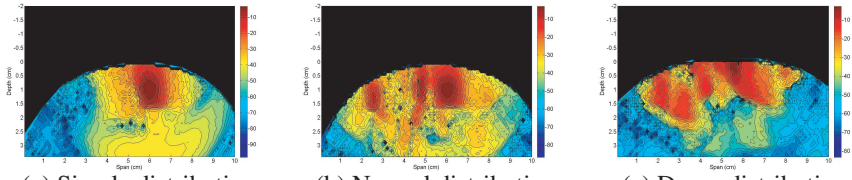

(a) Simple distribution (b) Normal distribution (c) Dense distribution

Figure 10. Images created by the Improved Delay and Sum (IDAS) beamformer for the simple, normal and dense fibroglandular tissue distributions, with a 5 mm tumour centered at location (1.5, 6.0).

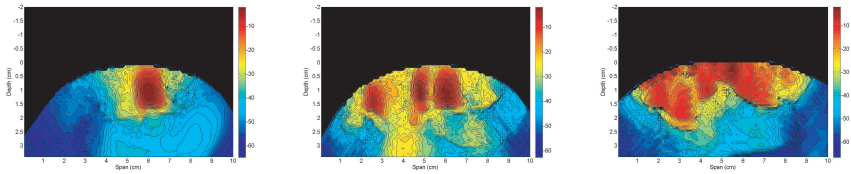

(a) Simple distribution (b) Normal distribution (c) Dense distribution

Figure 11. Images created by the Delay, Multiply and Sum (DMAS) beamformer for the simple, normal and dense fibroglandular tissue distributions, with a 5 mm tumour centered at location (1.5, 6.0).

Table 4. Average S/M and S/C ratios (in dBs) for each beamformer across the Simple (S), Normal (N) and Dense (D) fibroglandular distribution.

Beamformer	S/M (S)	S/M (N)	**S/M (D)**	S/C (S)	S/C (N)	**S/C (D)**
DAS	16.7298	10.9146	**3.7909**	20.6917	17.6149	**14.0347**
IDAS	33.6673	21.2130	**6.4597**	40.0991	32.0474	**19.5986**
DMAS	38.4475	21.6646	**3.2395**	43.0505	32.1205	**18.1061**

the coherence of the backscattered signals from the tumour after time-alignment, and therefore their effectiveness is markedly reduced where there is a significant difference between the assumed homogenous channel model and the actual heterogeneous breast.

6. CONCLUSION

UWB beamformers for the early detection of breast cancer were based on several assumptions, including the assumption that breast is primarily dielectrically homogeneous and that the dielectric

properties of normal tissue is such that constructive addition of UWB backscattered signals is possible. Based on Lazebnik's dielectric data, it appears that the dielectric contrast between normal and cancerous breast tissue had previously been over-estimated, while the dielectric heterogeneity of normal breast tissue had been considerably under-estimated. Both the IDAS and DMAS significantly outperform the DAS beamformer where the breast is mainly composed of adipose tissue and is primarily dielectrically homogeneous. However, in the more dense model, where fibroglandular tissue contributes to a significant mismatch between the assumed and actual channel propagation models, the improved performance promised by both IDAS and DMAS is significantly reduced. Furthermore, in the dense model the presence and location of the tumour is much more difficult to establish in the images created all beamformers. This prompts the development of more sophisticated beamformers to compensate for the more challenging imaging environment of the dielectrically heterogeneous breast.

ACKNOWLEDGMENT

This work is supported by Science Foundation Ireland under grant number 07/RFP/ENEF420.

REFERENCES

1. Nass, S. L., I. C. Henderson, and J. C. Lashof, *Mammography and Beyond: Developing Technologies for the Early Detection of Breast Cancer*, National Academy Press, 2001.
2. Lazebnik, M., L. McCartney, D. Popovic, C. B. Watkins, M. J. Lindstrom, J. Harter, S. Sewall, A. Magliocco, J. H. Booske, M. Okoniewski, and S. C. Hagness, "A large-scale study of the ultrawideband microwave dielectric properties of normal breast tissue obtained from reduction surgeries," *Phys. Med. Biol.*, Vol. 52, 2637–2656, 2007.
3. Lazebnik, M., D. Popovic, L. McCartney, C. B. Watkins, M. J. Lindstrom, J. Harter, S. Sewall, T. Ogilvie, A. Magliocco, T. M. Breslin, W. Temple, D. Mew, J. H. Booske, M. Okoniewski, and S. C. Hagness, "A large-scale study of the ultrawideband microwave dielectric properties of normal, benign and malignant breast tissues obtained from cancer surgeries," *Phys. Med. Biol.*, Vol. 52, 6093–6115, 2007.
4. Chaudhary, S. S., R. K. Mishra, A. Swarup, and J. M. Thomas,

"Dielectric properties of normal and malignant human breast tissue at radiowave and microwave frequencies," *Indian J. Biochem. Biophys.*, Vol. 21, 76–79, 1994.

5. Surowiec, A. J., S. S. Stuchly, J. R. Barr, and A. Swarup, "Dielectric properties of breast carcinoma and the surrounding tissues," *IEEE Trans. Biomed. Eng.*, Vol. 35, No. 4, 257–263, 1988.
6. Joines, W., Y. Zhang, C. Li, and R. L. Jirtle, "The measured electrical properties of normal and malignant human tissues from 50 to 900 MHz," *Med. Phys.*, Vol. 21, 547–550, 1993.
7. Campbell, A. M. and D. V. Land, "Dielectric properties of female human breast tissue measured in vitro at 3.2 GHz," *Phys. Med. Biol.*, Vol. 37, 193–210, 1992.
8. Meaney, P. M., M. W. Fanning, D. Li, S. P. Poplack, and K. D. Paulsen, "A clinical prototype for active microwave imaging of the breast," *IEEE Trans. Microwave Theory Tech.*, Vol. 48, 1841–1853, 2000.
9. Hagness, S. C., A. Taove, and J. E. Bridges, "Two-dimensional FDTD analysis of a pulsed microwave confocal system for breast cancer detection: Fixed focus and antenna array sensors," *IEEE Trans. Biomed. Eng.*, Vol. 45, 1470–1479, 1998.
10. Fear, E. C. and M. A. Stuchly, "Three-dimensional FDTD analysis of a pulsed microwave confocal system for breast cancer detection: Design of an antenna array element," *IEEE Trans. Antennas and Propagat.*, Vol. 47, 783–791, May 1999.
11. Nilavalan, R., S. C. Hagness, and B. D. V. Veen, "Numerical investigation of breast tumour detection using multi-static radar," *IEE Electronic Letters*, Vol. 39, No. 25, 1787–1789, Dec. 2003.
12. Lim, H., N. Nhung, E. Li, and N. Thang, "Confocal microwave imaging for breast cancer detection: Delay-multiply-and-sum image reconstruction algorithm," *IEEE Trans. Biomed. Eng.*, Vol. 55, No. 6, Jun. 2008.
13. Klemm, M., I. J. Craddock, J. A. Leendertz, A. Preece, and R. Benjamin, "Improved delay-and-sum beamforming algorithm for breast cancer detection," *International Journal of Antennas and Propagation*, Vol. 2008, 2008.
14. Liand, X. and S. C. Hagness, "A confocal microwave imaging algorithm for breast cancer detection," *IEEE Microwave and Wireless Components Letters*, Vol. 11, 130–132, 2001.
15. Lazebnik, M., M. Okoniewski, J. Booske, and S. Hagness, "Highly accurate debye models for normal and malignant breast tissue dielectric properties at microwave frequencies," *IEEE Microwave*

and Wireless Components Letters, Vol. 17, No. 12, 822–824, Dec. 2007.

16. Gabriel, C., S. Gabriel, and E. Corthout, "The dielectric properties of biological tissues: I. Literature survey," *Phys. Med. Biol.*, Vol. 41, 2231–2249, 1996.
17. Gabriel, S., R. W. Lau, and C. Gabriel, "The dielectric properties of biological tissues: II. Measurements in the frequency range 10 Hz to 20 GHz," *Phys. Med. Biol.*, Vol. 41, 2251–2269, 1996.
18. Bond, E. J., X. Li, S. C. Hagness, and B. D. V. Veen, "Microwave imaging via space-time beamforming for early detection of breast cancer," *IEEE Trans. Antennas and Propagat.*, 1690–1705, 2003.
19. Fear, E. C. and M. Okoniewski, "Confocal microwave imaging for breast tumor detection: Application to a hemispherical breast model," *2002 IEEE MTT-S International Microwave Symposium Digest*, Vol. 3, 1759–1763, 2002.
20. Fear, E. C., X. Li, S. C. Hagness, and M. A. Stuchly, "Confocal microwave imaging for breast cancer detection: Localization of tumors in three dimensions," *IEEE Trans. Biomed. Eng.*, Vol. 47, 812–812, 2002.